Lifetime measurements of first excited states in ^{16,18}C

H. J. Ong,[1,2,*] N. Imai,[2,†] D. Suzuki,[1] H. Iwasaki,[1,‡] H. Sakurai,[1,§] T. K. Onishi,[1] M. K. Suzuki,[1] S. Ota,[3] S. Takeuchi,[2] T. Nakao,[1] Y. Togano,[4] Y. Kondo,[5,§] N. Aoi,[2] H. Baba,[2] S. Bishop,[2] Y. Ichikawa,[1] M. Ishihara,[2] T. Kubo,[2] K. Kurita,[4] T. Motobayashi,[2] T. Nakamura,[5] T. Okumura,[5] and Y. Yanagisawa[2]

[1]*Department of Physics, University of Tokyo, Hongo 7-3-1, Bunkyo, Tokyo 113-0033, Japan*

[2]*RIKEN Nishina Center, Hirosawa 2-1, Wako, Saitama 351-0198, Japan*

[3]*Center for Nuclear Study, University of Tokyo, RIKEN campus, Hirosawa 2-1, Wako, Saitama 351-0198, Japan*

[4]*Department of Physics, Rikkyo University, Nishi-Ikebukuro 3-34-1, Toshima, Tokyo 171-8501, Japan*

[5]*Department of Physics, Tokyo Institute of Technology, Ookayama 2-12-1, Meguro, Tokyo 152-8551, Japan*

(Received 26 November 2007; revised manuscript received 5 June 2008; published 10 July 2008)

The electric quadrupole transition from the first 2^+ state to the ground 0^+ state in ^{18}C was studied through a lifetime measurement by an upgraded recoil shadow method applied to inelastically scattered radioactive ^{18}C nuclei. The measured mean lifetime is $18.9 \pm 0.9(\text{stat}) \pm 4.4(\text{syst})$ ps, corresponding to a $B(E2; 2_1^+ \rightarrow 0_{\text{g.s.}}^+)$ value of $4.3 \pm 0.2 \pm 1.0\, e^2$ fm^4, or about 1.5 Weisskopf units. The mean lifetime of the first 2^+ state in ^{16}C was remeasured to be $18.3 \pm 1.4 \pm 4.8$ ps, about four times shorter than the value reported previously. The discrepancy between the two results was explained by incorporating the γ-ray angular distribution measured in this work into the previous measurement. These transition strengths are hindered compared to the empirical transition strengths, indicating that the anomalous hindrance observed in ^{16}C persists in ^{18}C.

DOI: 10.1103/PhysRevC.78.014308 PACS number(s): 23.20.Js, 21.10.Tg, 27.20.+n, 29.30.Kv

I. INTRODUCTION

Structure of neutron-rich nuclei is one of the frontiers in nuclear physics. In such nuclei, several exotic phenomena such as a halo [1] or skin [2] structure and the disappearance of the traditional magic numbers [3–5] have been discovered with the advance of experimental techniques and accelerators. These findings are unexpected by the conventional nuclear structure models, hence require the renovation of the theory.

Recently, we reported another exotic phenomenon of extremely suppressed $B(E2)$ value for the transition between the first $2^+(2_1^+)$ state to the ground $(0_{\text{g.s.}}^+)$ state in neutron-rich ^{16}C [6]. The $B(E2)$ was obtained by measuring the mean lifetime of the 2_1^+ state $(\tau(2_1^+))$ using a new experimental technique. In general, an even-even atomic nucleus tends to exhibit global behavior of a quantum liquid drop, wherein the $B(E2)$ is inversely proportional to the excitation energy of the 2_1^+ state $(E(2_1^+))$ [7]. However, the measured $B(E2)$ of ^{16}C was found to deviate greatly from the value expected by the empirical formula [8] of the $E(2_1^+)$, indicating a suppressed proton collectivity in ^{16}C.

Contrary to the suppressed proton collectivity, a large neutron collectivity was suggested based on the measurement of the interference between the nuclear and electromagnetic interactions in the excitation from the ground state to the 2_1^+ state [9]. Indeed, a large quadrupole deformation length was observed in a recent work on the proton inelastic scattering [10], revealing that the neutrons predominantly contribute to the strength of the excitation to the 2_1^+ state whereas the protons seem to be frozen.

The suppressed $B(E2)$ may indicate quenched effective charges and/or the emergence of a new magic number $Z = 6$ in the light neutron-rich carbon isotopes. For neutron-rich nuclei with weakly-bound neutron(s), the core polarization is likely to be weakly induced. This effect together with the effect of large isospin gives rise to quenched core polarization charges [11,12], in particular, a small neutron effective charge that reduces the contribution of the valence neutron(s) to the $B(E2)$ value. Indeed, the quenched effective charges have been observed in the neighboring ^{15,17}B nuclei [13,14]. Moreover, in the case of the closed shell nuclei, the $B(E2)$ value will also be reduced. In this context, we note that the emergence of the proton magic number $Z = 6$ has been suggested by a shell model calculation [15].

Besides the shell model calculation, several other microscopic models have also been proposed to explain the mechanism of the small $B(E2)$ value for ^{16}C. A calculation using antisymmetrized molecular dynamics (AMD) has attributed the anomalous feature to the opposite deformations in the proton and the neutron matters [16,17]. It is interesting to note that calculations assuming a simple structure that ^{16}C is composed of $^{14}\text{C} + n + n$ have also reproduced the $E(2_1^+)$ and the $B(E2)$ of this nucleus [18–20]. To shed light on the exotic phenomenon exhibited by ^{16}C and to scrutinize the claim for the emergence of the $Z = 6$ magic number in the neutron-rich C isotope, more experimental information specifically on the neighboring ^{18}C isotope is awaited.

In this article, we report on the first lifetime measurement for the 2_1^+ state in ^{18}C populated via inelastic scattering of a

*onghjin@ribf.riken.jp; Present address: RCNP, Osaka University, Mihogaoka 10-1, Ibaraki, Osaka 567-0047, Japan.

†Present address: KEK, Oho 1-1, Tsukuba, Ibaraki 305-0801, Japan.

‡Present address: Institut für Kernphysik, Universität zu Köln, Köln, Germany.

§Present address: RIKEN Nishina Center, Hirosawa 2-1, Wako, Saitama 351-0198, Japan.

 ©2008 The American Physical Society

79-MeV/nucleon ^{18}C beam on a ^{9}Be target. The $\tau(2_1^+)$ value of ^{18}C is expected to be as long as that for ^{16}C since their energy level schemes are almost identical. Specifically, the $E(2_1^+)$ values are 1766 [21] and 1585(10) keV [22]; the one-neutron separation energies (S_n) are 4250(4) and 4180(30) keV, for ^{16}C and ^{18}C, respectively [21]. In the present work, lifetime measurements were extended to the 2_1^+ state of ^{16}C, thereby reexamining the previous result reported in Ref. [6]. In these measurements, the 2_1^+ state was populated through two different reactions, namely, inelastic scattering of ^{16}C on ^{9}Be at 72 MeV/nucleon and breakup reaction of ^{18}C at 79 MeV/nucleon. Moreover, the γ-ray angular distribution was measured for the 2_1^+ state produced in the ^{16}C inelastic scattering at 40 MeV/nucleon, with an aim to incorporate the distribution in an improved analysis of the previous data [6] taken at the same reaction energy. In addition, measurements were also performed for known lifetimes of the excited $1/2^-$ state in ^{11}Be and 3^- state in ^{16}N, produced through breakup reaction of ^{18}C, to verify the method.

The lifetime measurements were performed by means of the recoil shadow method (RSM), which was first applied to our previous work on ^{16}C [6]. In this method, the lifetime is determined by observing the emission-point distribution of γ rays emitted in flight from excited nuclei produced in inverse-kinematics reactions of incident radioactive projectiles. In the present work, we have upgraded the RSM to enhance both the efficiency and the accuracy of the measurement. The upgraded scheme thus employed involved a large array of NaI(Tl) detectors as well as a novel procedure that enables determination of lifetimes independent of the γ-ray anisotropy, which is to arise from nuclear spin alignment.

The present article is organized as follows. In Sec. II, we describe the principle and upgrade of the RSM. Details on the experiment are given in Sec. III. In Sec. IV, a brief description on Monte Carlo simulations, which were used to determine the mean lifetimes, is given. The results of the lifetime measurements with the upgraded RSM as well as that of reanalyzed data in Ref. [6] are presented in Sec. V. In Sec. VI, we discuss the $B(E2)$ values of ^{16,18}C. Finally, a summary is given in Sec. VII.

II. RECOIL SHADOW METHOD (RSM)

For earlier works on the recoil shadow method (RSM), we refer the reader to Refs. [23–26]. In both the previous [6] and the present works, we applied the RSM to γ decays from the excited radioactive nuclei. The RSM makes use of the shadow effect of a lead shield placed around a reaction target on NaI(Tl) detectors of a highly segmented and highly efficient γ-ray detector array. In this method, excited nuclei in flight are produced via inverse-kinematics inelastic scattering or fragmentation process induced by a radioactive nuclear beam (RNB) at intermediate energies. Each nucleus then travels a certain distance before decaying through emission of a γ ray, which is detected by the NaI(Tl) detector array. The yield of the γ rays detected by each NaI(Tl) detector depends on (a) the velocity ($\beta = v/c$) of the ejectile, (b) the emission point of the deexcitation γ ray, and (c) the γ-ray angular distribution in the rest frame of the ejectile. The angular distribution is governed by the alignment produced by the nuclear reaction [27]; the emission point depends on β of the ejectile (which is known) and the lifetime of the excited state. Hence, assuming that we know the angular distribution of the γ rays, the lifetime can be determined, in principle, by observing the yield distribution of the γ rays. For lifetimes of as short as a few tens of picoseconds, however, the yield distribution is not sensitive to the small variation of the emission point. Hence, determination of such lifetimes is achieved with the presence of the lead shield, which enhances the lifetime dependence of the yield distribution.

In the previous work [6], we bombarded a ^{9}Be target with a 40-MeV/nucleon ^{16}C beam and detected the deexcitation γ rays with only two layers of NaI(Tl) detectors placed cylindrically around the beam axis. The mean lifetime was determined by comparing the ratio between the γ-ray yields detected in the two layers with a calculated ratio function, which was obtained for several mean lifetimes through simulations. However, the angular distribution of the γ rays was not measured, and thus we had assumed the angular distribution obtained by a theoretical calculation, which imposed an extra uncertainty, in the simulation.

In this work, we have made three improvements to the RSM. First, we determined the lifetimes independent of the angular distribution. For the determination of each lifetime, two measurements of the γ-ray yields were performed: one with the lead shield installed, and the other without the lead shield. The γ-ray yield from the former measurement carries the information of both the lifetime and the γ-ray angular distribution, while that from the latter measurement carries mainly the information of the angular distribution. Hence, we can determine the lifetime by comparing the ratio of the two γ-ray yields to a simulated ratio function. Second, we compensated the drop (by almost two orders of magnitude) in the beam intensity from ^{16}C to ^{18}C by increasing the number of detectors from 32 in the previous setup to 130. The last improvement was achieved by using a fast ^{18}C beam at an energy of about 79 MeV/nucleon, thus increasing the mean decay length by a factor of about 1.4. It is worth noting that incorporation of intermediate-energy RNB with $\beta = 0.3$–0.4 in the RSM facilitates measurements of lifetimes of down to about 10 ps. As will be shown later, the results for ^{11}Be and ^{16}N demonstrate that the present RSM is a reliable and powerful means to determine the lifetimes of nuclear excited states with simple or known γ-decay schemes. Because the present RSM is independent of the γ-ray angular distribution, it can be used to measure lifetimes of as short as about 10 ps of excited states produced by any kind of reaction channels with the intermediate-energy RNB in a single experiment. In fact, we have also successfully measured the lifetimes of excited states in ^{17}C, produced by one-neutron knockout reaction of ^{18}C [28].

III. EXPERIMENT

The experiment was performed at the RIKEN accelerator research facility. Secondary beams of ^{16,18}C were produced in

two separate measurements through projectile fragmentation of an 110-MeV/nucleon ^{22}Ne primary beam, and separated by the RIPS beam line [29]. Particle identification of the secondary beam was performed event-by-event by means of the time-of-flight (TOF)-ΔE method using two 1.0-mm-thick plastic scintillation counters located at the second and final focal planes of RIPS. The ^{16,18}C beams with energies of 72 MeV/nucleon and 79 MeV/nucleon, respectively, were directed at a 370-mg/cm^2 ^{9}Be target placed at the exit of the RIPS beam line. In the case of the measurement of the γ-ray angular distribution for the data in Ref. [6], the energy of the ^{16}C beam was further reduced to 40 MeV/nucleon by using a 6-mm-thick aluminum degrader. Two sets of parallel plate avalanche counters (PPACs) were placed upstream of the target to measure the position and angle of the projectile incident upon the target. The ^{16,18}C beam had typical intensities of 6.5×10^4 and 2.3×10^4 particles per second, respectively.

Outgoing particles from the target were identified by the ΔE-E-TOF method using a plastic scintillator hodoscope [30] located 3.8 m downstream of the target. The hodoscope, with an active area of 1.0×1.0 m^2, consisted of thirteen vertical ΔE-scintillator slats and sixteen horizontal E-scintillator bars with 5.0 mm and 60.0 mm thicknesses, respectively. The hodoscope was placed symmetrically perpendicular to the beam axis. Scattering angles were determined by combining the hit position information on the hodoscope with the incident angles and hit positions on the target obtained by the PPACs.

In order to implement the RSM concept, a thick γ-ray shield was placed around the target, as shown in Fig. 1. The shield was a 5 cm-thick lead block with an outer frame of 24×24 cm^2 and an inner hole of 5.4 cm in diameter. The inner hole surrounded the beam tube housing the ^{9}Be target. We removed the lead shield during measurement of the angular distribution of γ rays. For the sake of later discussion, the z-axis is defined as the beam direction, which is close to the flight direction of the deexciting nucleus. The origin of the z-axis, $z = 0.00$ cm, was taken at the upstream edge of the lead shield. We have carried out both measurements, namely, the measurements with and without the lead shield, with the target placed at $z = -0.15$ cm and $z = 2.05$ cm. We refer to these setups as the "upstream setup" and the "center setup" hereinafter.

The γ rays from the excited nuclei in-flight were detected by an array of 130 NaI(Tl) detectors, which form part of the DALI1 [31] and the DALI2 [32]. The NaI(Tl) detectors, all of which are rectangular in shape, are of three different sizes: $4.5 \times 8 \times 16$ cm^3, $4 \times 8 \times 16$ cm^3, $6.1 \times 6.1 \times 12.2$ cm^3. The array was divided into 10 layers, labeled L1–10 as shown in Fig. 1, with each layer consisting of $10 \sim 18$ detectors arranged coaxially with respect to the beam direction. The layers are closely packed to cover polar angular ranges of $15^\circ \sim 85^\circ$ and $100^\circ \sim 170^\circ$ in the laboratory frame. The detectors were mounted on and supported by nine 3-mm-thick aluminum plates. The distances of the center of the detectors from the center of the Be target ranged from 28 cm to 56 cm.

In the present work, we counted the number of full-energy-peak events detected by each layer during the measurements with and without the lead shield. For convenience, the numbers obtained with the ith layer during the former and the latter measurements are denoted by $N^i_{\rm wPb}$ and $N^i_{\rm woPb}$. The $N^i_{\rm wPb}$ and

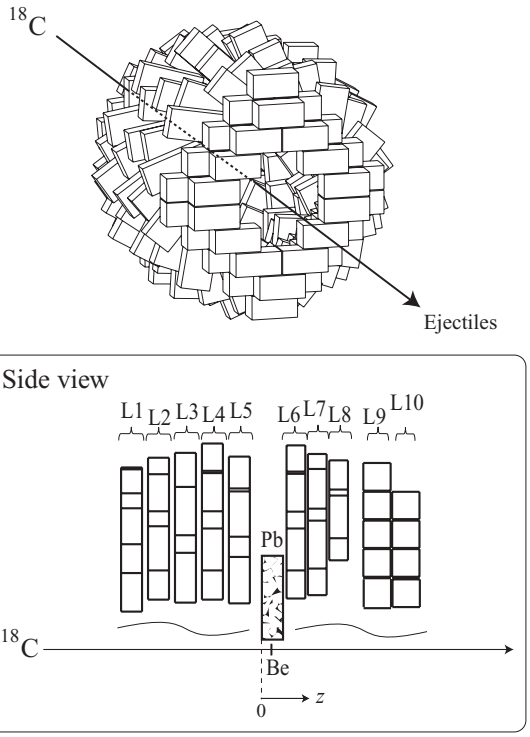

FIG. 1. Schematic view of γ-ray detectors. A beryllium target is surrounded by a 5 cm-thick lead shield, and ten layers of NaI(Tl) scintillators (L1 $\sim$ L10) placed cylindrically around the beam axis. For clarity, only part of the detectors and lead shield is shown in the inset.

$N^i_{\rm woPb}$ were obtained by fitting the measured γ-ray energy spectra with response functions obtained with simulations, plus γ-ray spectra for the ^{14}C isotope as backgrounds. The spectra for ^{14}C were selected because (i) all excited states in ^{14}C lie at energies above 6 MeV, and there is no significant γ line around 1.6 MeV, (ii) the ^{14}C isotope was produced through projectile fragmentation reaction of the ^{18}C (or ^{16}C) in the secondary target, and as such its "background spectrum" resembles that of for ^{18}C (or ^{16}C).

As mentioned earlier, a key point of the present work is the elimination of the dependence of the measured lifetime on the γ-ray angular distribution. For this purpose, we determined the deficiency of the γ-ray yields due to the lead shield. The deficiency (D^i) of the i-th layer detectors is defined as the ratio between the yields detected with and without the shield, i.e.,

$$D^i = f_b N^i_{\rm wpb}/N^i_{\rm wopb}, \quad (1)$$

where f_b is the normalization factor for different total number of beam particles in the two measurements. The lifetime was determined by comparison of the measured deficiency ($D^i_{\rm exp}$) with the simulated one ($D^i_{\rm sim}$).

IV. MONTE CARLO SIMULATIONS

The simulated deficiency of each layer as a function of various lifetime for the respective deexcitation γ rays was obtained by performing Monte Carlo simulations using the

GEANT code [33]. We have taken into account the geometry of the experimental setup, including the shape of the detectors, in the simulations. The geometry was checked by performing separate measurements in which ^{137}Cs, ^{22}Na, and ^{60}Co standard sources emitting 662-keV, 1275-keV, 1173-keV, and 1333-keV γ rays were placed at several positions from $z = -0.15$ to 5.15 cm. The deficiencies of all layers measured for the respective target position were reproduced by the simulation within accuracies of $\pm 3\%$ and $\pm 7\%$ for layers with $D^i_{\rm exp} \geqslant 0.2$ and $D^i_{\rm exp} < 0.2$, respectively.

The simulation was then applied to the case of γ-rays emitted from the deexciting particles in flight. For this simulation, we have considered the experimentally obtained parameters such as the energy and emittance (angular spread $\sim$10 mrad in rms in directions perpendicular to the beam axis and beam spot size $\sim$10 mm in rms on the target) of the projectile, the angular spread (as large as $\lesssim 14^\circ$ for the case of the ^{16}C beam at 40 MeV/nucleon) due to reaction and multiple scattering, and the energy loss in the target. Apart from determining the $D^i_{\rm sim}$, the response functions obtained from the simulation were also used for the fitting of the experimental γ-ray energy spectra. Note that the strong dependence of $D^i_{\rm sim}$ on the lifetime is exhibited in Figs. 3, 5, 7, and 9.

V. RESULTS

We deduced the $D^i_{\rm exp}$ using Eq. (1) and determined the lifetimes for the respective excited states. In the case of the inelastic scattering with the 40-MeV/nucleon ^{16}C beam, we revised the lifetime of the 2^+_1 state reported previously [6] by incorporating the measured γ-ray angular distribution. The results from these measurements are presented.

A. Lifetime of 2^+_1 state in ^{18}C

We show in Fig. 2 the γ-ray energy spectrum measured with the L6 NaI(Tl) detectors, which were located at polar angle of about 90° in the rest frame of the ^{18}C ejectile. The spectrum was obtained with the center setup and without the lead shield. The significant peak around 1500 keV corresponds to the 1585-keV line from the $2^+_1 \rightarrow 0^+_{\rm g.s.}$ transition, while the minor peak around 1000 keV corresponds to the 919-keV line from the transition between the 2504-keV excited state and the 2^+_1 state. The level scheme for ^{18}C as shown in the inset of Fig. 2 has been proposed recently based on the in-beam γ-spectroscopy [22]. The two γ lines observed correspond to the transitions shown by the bold arrows in the level scheme. The two significant peaks around 200 keV and 300 keV are from the known transitions in ^{17}C [22,28,34]; the γ-ray energies shown are taken from Ref. [28].

By considering the sum spectrum of all detectors, the cascade contribution from the second excited state to the 2^+_1 state was determined to be about 9% relative to the $2^+_1 \rightarrow 0^+_{\rm g.s.}$ transition. Since the error that might arise from the cascade contribution is negligibly small compared to the systematic error mentioned below, we have neglected the cascade contribution in our analysis.

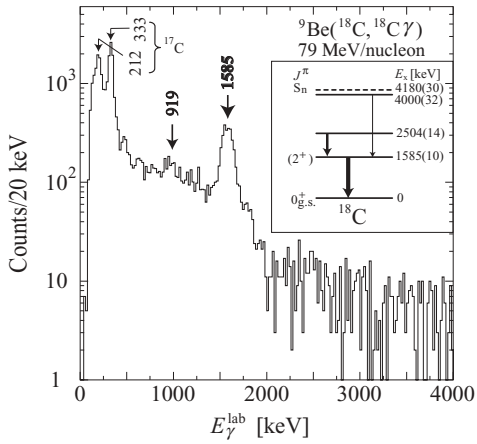

FIG. 2. γ-ray energy spectrum for the inelastic scattering of the 79-MeV/nucleon ^{18}C nuclei on ^{9}Be. The γ rays were detected by the L6 NaI(Tl) detectors. The inset shows the energy level scheme of ^{18}C and the known γ-ray transitions [22].

The simulated deficiencies were obtained for several assumed mean lifetimes ranging from $\tau(2^+_1) = 0$ ps to 40 ps. As an example, we compare the $D^i_{\rm exp}$ value with the $D^i_{\rm sim}$ values obtained for $\tau(2^+_1) = 0$, 20, and 40 ps. The $D^i_{\rm exp}$'s (filled and open circles) and the $D^i_{\rm sim}$'s for $\tau(2^+_1) = 0$ ps (dashed line), 20 ps (solid line), and 40 ps (dotted line) are plotted in Fig. 3 for the (a) center and (b) upstream setups. Note that we have omitted the experiment data for the layers with $N^i_{\rm wPb} \approx 0$, which do not contribute to the determination of the mean lifetime. The figures indicate that the mean lifetime of the 2^+_1 state locates around 20 ps. The mean lifetime was determined by searching the χ^2 minimum; the $\chi^2(\tau)$ is given by

$$\chi^2(\tau) = \sum_i \frac{\left(D^i_{\rm exp} - D^i_{\rm sim}(\tau)\right)^2}{\left(\delta D^i_{\rm exp}\right)^2}, \qquad (2)$$

where the $\delta D^i_{\rm exp}$ represents the statistical error. The χ^2 distributions for $\tau(2^+_1)$ from 0 ps to 40 ps, as shown in the inset of Fig. 3, give $\tau(2^+_1) = 19.9 \pm 1.0$ ps and 14.9 ± 2.1 ps for the center and upstream setups, respectively. We adopted the weighted mean of these two values, 18.9 ± 0.9 ps, as the mean lifetime for the 2^+_1 state in ^{18}C.

The systematic error was mainly due to (a) the uncertainty of the target position, about 0.5 mm in the beam direction, and (b) the discrepancy between the measured deficiency and the simulated one. The uncertainty in the target position, which corresponds to the uncertainty in the emission point, resulted in an uncertainty of about 4.4 ps for the ^{18}C ejectiles traveling at about 38% of the speed of light. The error due to "(b)" was estimated to be 0.5 ps by changing the $D^i_{\rm sim}(\tau)$ randomly within $\pm 3\%$ (or $\pm 7\%$) and observing the deviation of the lifetime thus obtained. Other possible sources of systematic error we have considered but neglected are the beam parameters such as the beam spot size, and the incident and scattering angles. The uncertainty in the beam position on the target was about 4 mm, while the angular resolutions of the incident and scattering angles were about 2 mrad and 3 mrad, respectively. We note that even assuming a pointed beam (which is of course

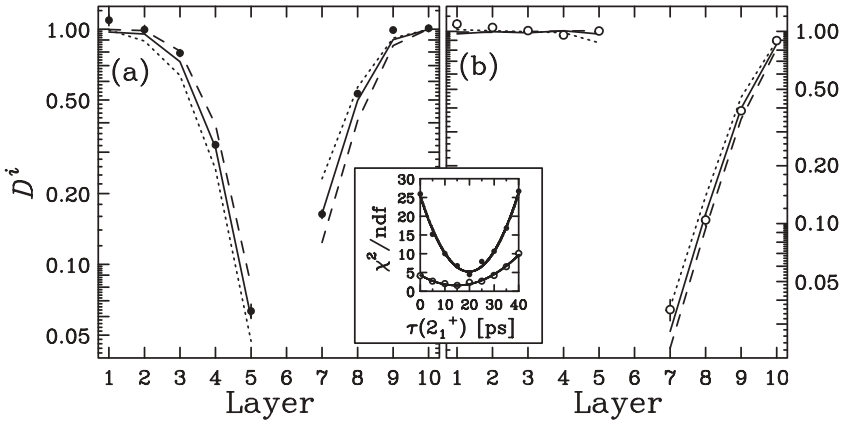

FIG. 3. The $D^i_{\rm exp}$'s, denoted by the filled and open circles, of the respective layers for the $2^+_1 \rightarrow 0^+_{\rm g.s.}$ transition in ^{18}C as compared with the simulated values. The dashed, solid and dotted lines represent the $D^i_{\rm sim}$ values calculated for $\tau(2^+_1) = 0$, 20, and 40 ps, respectively. (a) The D^i distribution for the center setup. (b) The D^i distribution for the upstream setup. The inset shows the reduced χ^2 distributions as functions of $\tau(2^+_1)$ for the center (filled circles) and upstream (open circles) setups.

unlikely) in the simulation the determined mean lifetime only changed about 1.0 ps, which is negligible compared to the error due to the uncertainty in the target position. Similarly, the resultant uncertainty in the emission point due to the uncertainties of the incident and scattering angles was of the order of μm, which is again negligible. Hence, taking the root sum square of the errors from "(a)" and "(b)", the resultant systematic error was determined to be 4.4 ps. The mean lifetime thus obtained is 18.9 ± 0.9(stat) ± 4.4(syst) ps. For simplicity, the notations for the statistical (stat) and the systematic (syst) errors will be omitted from now onwards.

B. Lifetime of $1/2^-$ state in ^{11}Be

Figure 4 shows an example of the γ-ray energy spectrum measured with the L6 NaI(Tl) detectors in coincidence with the ^{11}Be ejectiles. The spectrum was obtained with the center setup and without the lead shield. Only one peak that corresponds to the transition of the $1/2^- \rightarrow 1/2^+$ is observed at around 300 keV. The $1/2^-$ state is the only known bound excited state that decays through γ transition as shown by the level scheme [21] in the inset of Fig. 4. The mean lifetime is $\tau(1/2^-) = 0.166(14)$ ps [21], which is much shorter than the mean lifetime of ^{18}C (2^+_1). By applying the RSM to this short lifetime, we verified the lower limit of the dynamic range of the method.

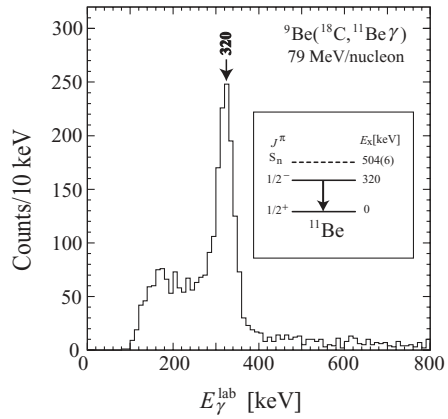

FIG. 4. γ-ray energy spectrum in coincidence with the ^{11}Be ejectiles. The γ rays were measured with the L6 NaI(Tl) detectors. The inset in the figure presents the energy level scheme and the lifetime of the first excited state of ^{11}Be.

The $D^i_{\rm exp}$ and the $D^i_{\rm sim}$ values for $\tau(1/2^-) = 0$, 15, and 30 ps are shown in Fig. 5 for the two different target positions. As is obvious from the plots, the deviation of the $D^i_{\rm sim}$ from the $D^i_{\rm exp}$ becomes larger with longer assumed mean lifetime. The simulated deficiencies for $\tau(1/2^-)$ ranging from 0 ps to 30 ps were used to obtain the χ^2 value as a function of $\tau(1/2^-)$. From the χ^2 distribution, the mean lifetimes were determined to be 3.5 ± 1.3 ps and 9.5 ± 2.8 ps for the center and the upstream setups, respectively. The weighted mean of the two values, i.e., 4.6 ± 1.1 ps was adopted.

The sources of the systematic error are similar to those of the case of ^{18}C. Nonetheless, it is sufficient to consider only the one due to the uncertainty in the target position of ± 0.5 mm, which was dominant. For the ^{11}Be ejectiles with $\beta \sim 0.37$, the associated uncertainty in the determined mean lifetime is about 4.5 ps. Thus, the resultant mean lifetime for the $1/2^-$ state is $4.6 \pm 1.1 \pm 4.5$ ps. This result is consistent with the reference value of 0.166(14) ps [21]. The large error shows that the RSM is not suitable for determination of the lifetime below 10 ps.

C. Lifetime of 3^- state in ^{16}N

The validity of the RSM was also tested by measuring the known lifetime of the 3^- state of ^{16}N. The excited 3^- state decays to the ground 2^- state with the mean lifetime of $\tau(3^-) = 132(2)$ ps [21]. The Doppler-corrected γ-ray energy spectrum measured by all NaI(Tl) detectors is shown in Fig. 6. A minor and a prominent peaks are observed around 400 keV and 300 keV, respectively. The 400-keV peak corresponds to the 397-keV γ line from the $1^- \rightarrow 2^-$ transition, while the 300-keV peak includes two γ lines of 277 keV and 298 keV from the $1^- \rightarrow 0^-$ and $3^- \rightarrow 2^-$ transitions, as shown by the level scheme [21] in the inset of Fig. 6.

As is evident from Fig. 6, the 277-keV and the 298-keV peaks were not resolved in the energy spectrum. Hence, to determine the $N^i_{\rm wopb}$ and $N^i_{\rm wpb}$ for the 298-keV peak, it was necessary to determine the contribution of the 277-keV line in the 300-keV peak. We determined the contribution by fitting the energy spectrum of all NaI(Tl) detectors with the simulated response function for the 298-keV γ line, and a combined

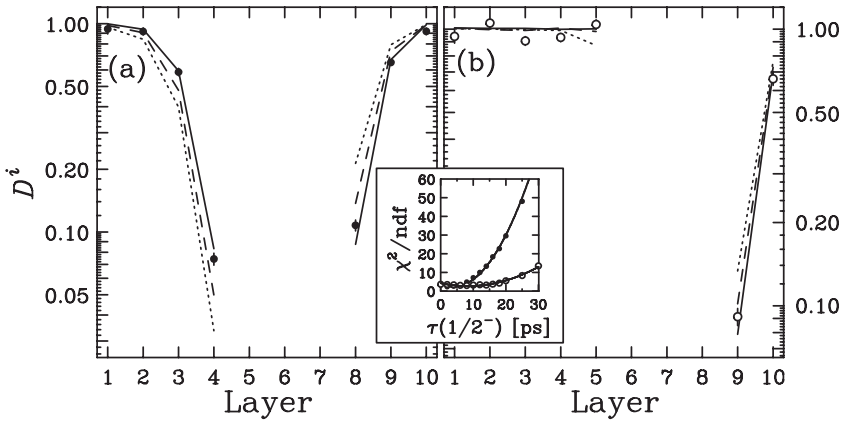

FIG. 5. The $D^i_{\rm exp}$'s, denoted by the filled and open circles, of the respective layers for the $1/2^- \rightarrow 1/2^+$ transition in ^{11}Be as compared with the simulated values. The solid, dashed and dotted lines represent the $D^i_{\rm sim}$ calculated for $\tau(1/2^-) = 0$, 15, and 30 ps, respectively. (a) The D^i distribution for the center setup. (b) The D^i distribution for the upstream setup. The inset shows the reduced χ^2 distributions as functions of $\tau(1/2^-)$ for the center (filled circles) and upstream (open circles) setups.

response function for the 277-keV and 397-keV lines, taking into account the branching ratio [21] of the decays from the 1^- state. The contribution of the 277-keV line was determined to be about 25%. By fixing the 277-keV contribution to 25%, we fitted the energy spectrum for each layer with the simulated response functions and the γ-ray spectrum for the ^{14}C isotope as background.

Figure 7 shows the $D^i_{\rm exp}$ and the $D^i_{\rm sim}$ values simulated for $\tau(3^-) = 100$, 140 and 180 ps for the two target positions. The plots clearly indicate that the lifetime locates around 140 ps. The simulated deficiencies for $\tau(3^-)$ ranging from 115 ps to 175 ps were used to obtain the χ^2 values as a function of $\tau(3^-)$. From the χ^2 distributions, we obtained $\tau(3^-) = 137 \pm 4$ ps and 136 ± 3 ps for the center and the upstream setups, respectively. The weighted mean of the two values thus obtained is 136 ± 3 ps.

Unlike the cases for ^{18}C and ^{11}Be, the systematic error is mainly due to the uncertainty in the determination of the 277-keV contribution in the 300-keV peak. This uncertainty, determined to be about 5%, is ascribed to the uncertainty in the energy calibration of the NaI(Tl) detectors, which was about 2 keV at 300 keV. The resultant systematic error distributes from -7 ps to $+11$ ps. Hence, the mean lifetime for the 3^- state was determined to be $136 \pm 3^{+11}_{-7}$ ps, which is in good agreement with the reference value of 132(2) ps [21].

We shall note that the energies of the γ rays emitted by ^{11}Be and ^{16}N are well below that of from the 2^+_1 state in ^{18}C, which is in the region of 1300–2300 keV depending on the layer. To rule out any possible energy dependence, we have also measured the mean lifetime of the 2^+_1 state in ^{12}B. The result is consistent with the value of 260 fs [21] given in the literature.

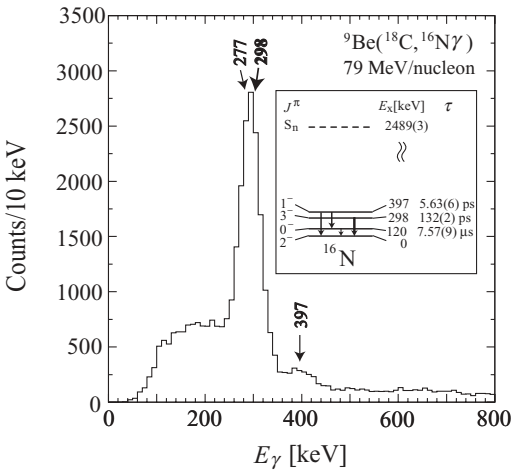

FIG. 6. Doppler corrected γ-ray energy spectrum in coincidence with the ^{16}N ejectiles. The γ rays were measured with all NaI(Tl) detectors. The inset shows the energy level scheme and the known mean lifetimes of the exited states in ^{16}N.

D. Lifetime of 2^+_1 state in ^{16}C revisited

1. Inelastic scattering of 72-MeV/nucleon ^{16}C beam

Figure 8(a) shows an example of the γ-ray energy spectrum in coincidence with the ^{16}C ejectiles obtained with the L6 NaI(Tl) detectors during the measurement with the center setup and without the lead shield. The significant peak around 1800 keV corresponds to the 1766-keV γ line from the $2^+_1 \rightarrow 0^+_{\rm g.s.}$ transition. The two peaks around 300 keV and the peak around 740 keV are from the known transitions in ^{17}C [22,28,34] and ^{15}C [21], respectively. The minor peak around 1000 keV, which was also observed at the same energy in the spectra of the other layers as well as in the spectra of other reaction channels, is likely to correspond to the 980.7-keV [21] line from ^{8}Li produced through fragmentation of the ^{9}Be reaction target. Although no notable peak can be observed around 2300 keV in the figure, the sum spectrum of all NaI(Tl) detectors exhibits a small peak, which corresponds to the cascade transition from the higher excited state(s) as shown by the energy level scheme [21] in the top right panel of Fig. 8. These higher excited states cannot be identified due to the resolution of the NaI(Tl) detectors. Nonetheless, by fitting the sum spectrum with a simulated response function for 2300-keV γ rays, the cascade contribution was determined to be 9% relative to the $2^+_1 \rightarrow 0^+_{\rm g.s.}$ transition. Similar to the case for ^{18}C, this cascade contribution is negligibly small, and thus was not considered in our analysis.

The experimental deficiency of each layer is compared with the simulated ones of $\tau(2^+_1) = 0$, 20, and 40 ps in Fig. 9 for the two target positions. The simulated curves ranging from $\tau(2^+_1) = 0$ ps to 40 ps were used to obtain the χ^2 values as a

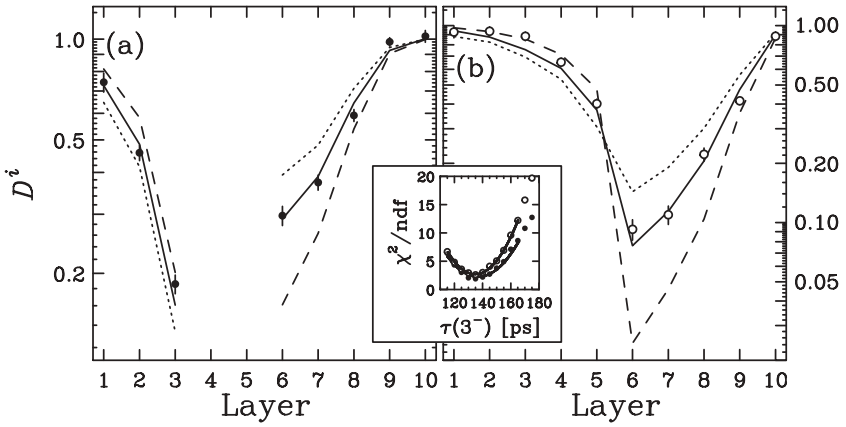

FIG. 7. The $D^i_{\rm exp}$'s, denoted by the filled and open circles, of the respective layers for the $3^- \rightarrow 2^-$ transition in ^{16}N as compared with the simulated values. The dashed, solid and dotted lines represent the $D^i_{\rm sim}$ calculated for $\tau(3^-) = 100$, 140, and 180 ps, respectively. (a) The D^i distribution for the center setup. (b) The D^i distribution for the upstream setup. The inset shows the reduced χ^2 distributions as functions of $\tau(3^-)$ for the center (filled circles) and upstream (open circles) setups.

function of $\tau(2^+_1)$. The χ^2 distributions give $\tau(2^+_1) = 18.3 \pm 1.8$ ps and 14.8 ± 3.9 ps for the center and the upstream setups, respectively. Taking the weighted mean of the two values, the mean lifetime was determined to be 17.7 ± 1.6 ps. This value is about four times shorter than the value reported previously [6].

The sources of the systematic error are similar to those for ^{18}C. Based on the same analysis, the systematic errors attributed to the uncertainties of the $D^i_{\rm sim}$ and the uncertainty of the target position were determined to be 0.5 ps and 4.6 ps, respectively. Adopting the root sum square of these two values as the systematic error, the mean lifetime thus obtained is $17.6 \pm 1.6 \pm 4.6$ ps.

2. *Breakup reaction of 79-MeV/nucleon ^{18}C beam*

Figure 8(b) shows the γ ray energy spectrum measured by the L6 NaI(Tl) detectors. The spectrum was obtained with the center setup and without the lead shield. A significant peak

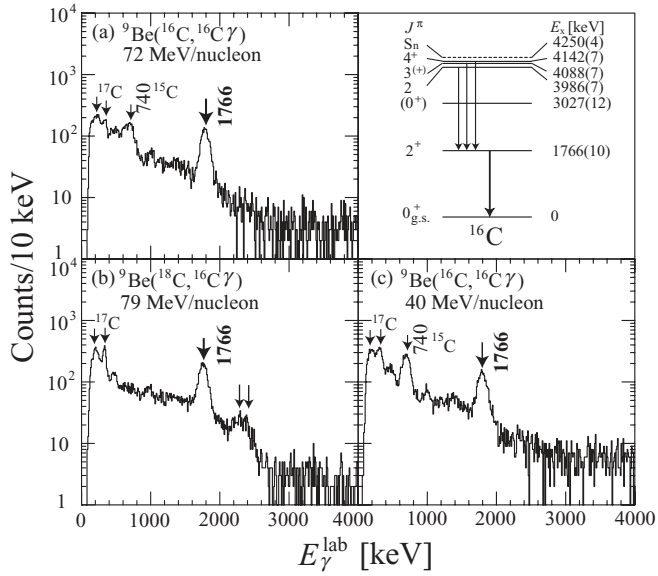

FIG. 8. γ-ray energy spectra for ^{16}C obtained with the L6 NaI(Tl) detectors during the measurement with the center setup and without the lead shield. (a) The inelastic scattering of ^{16}C at 72 MeV/nucleon. (b) The breakup reaction of ^{18}C to ^{16}C at 79 MeV/nucleon. (c) The inelastic scattering of ^{16}C at 40 MeV/nucleon. The level scheme with the known transitions in ^{16}C is shown in the top right panel.

around 1800 keV corresponds to the $2^+_1 \rightarrow 0^+_{\rm g.s.}$ transition of 1766 keV. Compared with the energy spectrum of the inelastic scattering, the cascade transition observed around 2300 keV was enhanced. By considering the sum spectrum for all NaI(Tl) detectors, the cascade contribution was determined to be 22% relative to the $2^+_1 \rightarrow 0^+_{\rm g.s.}$ transition.

In contrast to the case for inelastic channel, the cascade contribution was quite large. A possible sizable lifetime for the higher excited state(s) might affect the outcome of the lifetime determination for the 2^+_1 state. Hence, to determine the $\tau(2^+_1)$ and simultaneously take into account the cascade contribution, we carried out a minimization two-parameter χ^2 analysis. The χ^2 values were obtained with the measured $D^i_{\rm exp}$'s and the $D^i_{\rm sim}$'s. Here, the $D^i_{\rm sim}$'s were obtained for $\tau(2^+_1)$ and the lifetime of the higher excited state, denoted by τ(cascade) hereinafter, from 0 ps to 40 ps. A minimum was observed around $\tau(2^+_1) = 20$ ps and τ(cascade) $= 0$ ps. The mean lifetimes for the 2^+_1 state were determined to be 20.2 ± 3.3 ps and 16.9 ± 6.9 ps for the center and the upstream setups, respectively. Taking the weighted mean of the two values, we obtained $\tau(2^+_1) = 19.6 \pm 3.0$ ps.

The sources of the systematic error are similar to the ones for the inelastic channel. The error attributed to the uncertainties of the $D^i_{\rm sim}$'s is 0.5 ps. Meanwhile, the speed of the ^{16}C nuclei was about 37% of the speed of light. Hence, the systematic error ascribed to the uncertainty in the target position was about 4.5 ps. Taking these two systematic errors into consideration, the resultant mean lifetime for the breakup channel becomes $19.6 \pm 3.0 \pm 4.5$ ps. This value is consistent with the value determined from the inelastic channel.

3. *Inelastic scattering of 40-MeV/nucleon ^{16}C beam*

The deexcitation γ rays from the ^{16}C nuclei inelastically excited with the Be target were measured at 40 MeV/nucleon. Figure 8(c) shows the γ-ray energy spectrum measured with the L6 NaI(Tl) detectors. The spectrum was obtained with the center setup and without the lead shield. Since no notable peak was observed around 2300 keV, we have neglected the effect of the cascade contribution on the angular distribution of the $2^+_1 \rightarrow 0^+_{\rm g.s.}$ transition.

In the previous experiment [6], we determined the $\tau(2^+_1)$ value by comparing the relative yields of deexcitation γ rays

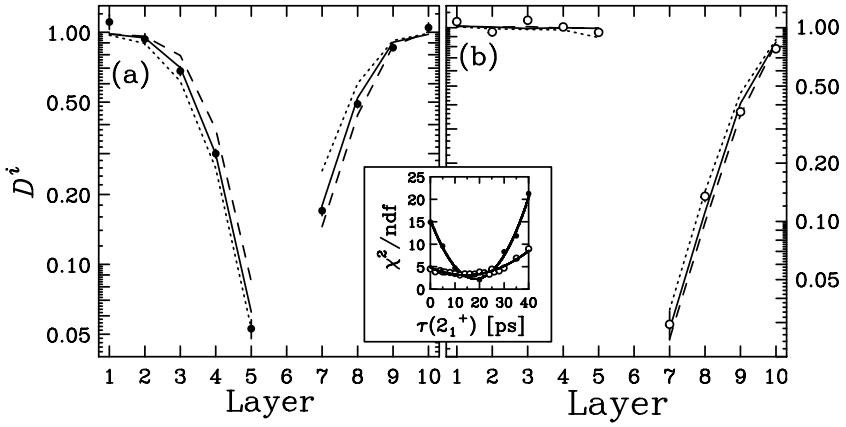

FIG. 9. Results for the inelastic scattering of 72-MeV/nucleon ^{16}C beam. The $D^i_{\rm exp}$'s, denoted by the filled and open circles, of the respective layers for the $2^+_1 \rightarrow 0^+_{\rm g.s.}$ transition in ^{16}C as compared with the simulated values. The dashed, solid and dotted lines represent the $D^i_{\rm sim}$ calculated for $\tau(2^+_1) = 0$, 20, and 40 ps, respectively. (a) The D^i distribution for the center setup. (b) The D^i distribution for the upstream setup. The inset shows the reduced χ^2 distributions as functions of $\tau(2^+_1)$ for the center (filled circles) and upstream (open circles) setups.

measured with two layers of NaI(Tl) detectors. Since the γ-ray yields depend on not only the shadow effect but also the angular distribution of γ rays, we assumed an angular distribution with a calculation. In the present work, we measured the angular distribution (without the lead shield) to determine the relative yields without the shadow effect. The angular distribution was obtained by fitting the energy spectrum of each layer with the corresponding simulated response function.

The layers in the previous experiment, labeled R1 and R2, were located just upstream of the target with central angles of 135° and 116° in the rest frame of the ^{16}C ejectile, respectively. The measured angular distribution of γ rays emitted from the 2^+_1 state is shown in Fig. 10, together with the calculated distributions obtained with the ECIS79 [35] code using two optical-model parameter sets, OM1 [36] and OM2 [37]. These calculated distributions were used to determine the $\tau(2^+_1)$ in the previous work. From the figure, it is obvious that the calculations fail to reproduce the experimental data, especially at around 90°. In order to determine the angular distribution quantitatively, we fitted the data with the following function:

$$W(\theta) = 1/(4\pi)(1 + aP_2(\cos\theta) + bP_4(\cos\theta)). \qquad (3)$$

The $P_{l;(l=2,4)}$ in the above function are the Legendre polynomials, while the a and b are the coefficients. The best-fitted result is shown in Fig. 10 by the solid curve. Note that the error bars in the figure are purely statistical; the systematic errors, which were mainly due to the simulation, were about 3%–5%. In the figure, the central angles of the detectors R1 and R2 are shown by the arrows, indicating that the corresponding $W(\theta)$ values are almost identical. The two-parameter fitting yielded $a = -0.22 \pm 0.06$ and $b = -0.48 \pm 0.07$, which gave $W(135°)/W(116°) = 1.00 \pm 0.02$. Although the errors of the fitting parameters were about 25% and 15%, respectively, the second and third terms in Eq. (3) were much smaller than the first term. As a result, the errors for $W(\theta)$ at the respective angles as well as that of $W(135°)/W(116°)$ were relatively small. On the other hand, the systematic errors due to the simulation only changed the $W(135°)/W(116°)$ value by 0.01 so that the overall uncertainty of $W(135°)/W(116°)$ remained at 0.02.

The calculated distributions yielded $W(135°)/W(116°) = 0.91$ for OM1 and 0.88 for OM2, which made the simulated R1/R2 ratio smaller. As a result, a longer mean lifetime was deduced. Figure 11 shows the simulated R1/R2 ratio as a function of $\tau(2^+_1)$ by incorporating the experimental angular distribution. The dashed lines represent the original simulated

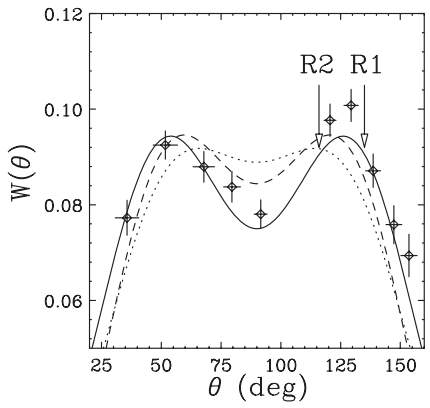

FIG. 10. The angular distribution of the deexcitation γ rays from the 2^+_1 state in ^{16}C, observed in the rest frame of the ^{16}C ejectile. The solid line indicates the best fitted angular distribution. The dashed and dotted lines represent the calculated distributions for OM1 and OM2, respectively.

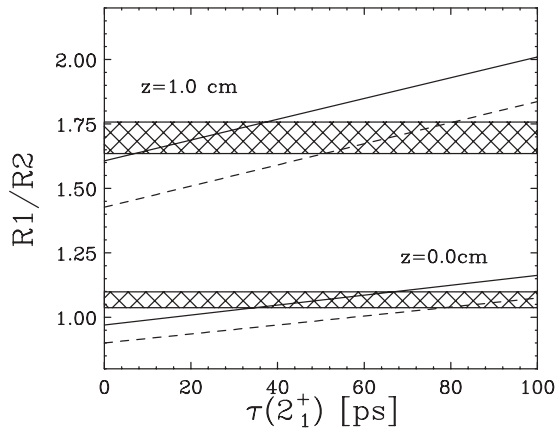

FIG. 11. Two solid lines represent $\tau(2^+_1)$ vs R1/R2 curves obtained by Monte Carlo simulation including the experimental angular distribution of deexcitation γ ray for target positions of $z = 0.0$ and 1.0 cm. The dashed lines represent the original simulated R1/R2 ratio [6]. The hatched zones represent the experimentally determined R1/R2 ratios [6] for the two target positions.

R1/R2 ratio. The R1/R2 ratio measured in the previous work for the two target positions, $z = 0.0$ and 1.0 cm, are shown by the hatched zones. The overlapped region between the experimental R1/R2 ratio and the simulated lines corresponds to 51 ± 21 ps and 20 ± 18 ps for $z = 0.0$, 1.0 cm, respectively. The resultant mean lifetime of 34 ± 14 was obtained by taking the weighted mean of these two values. The systematic uncertainties attributed mainly to the geometrical uncertainty and the uncertainty of $W(135^\circ)/W(116^\circ)$ were estimated to be 6.8 ps and 6.6 ps. We note that realistic evaluation of the latter systematic uncertainty was unavailable in the previous work due to the lack of angular distribution data. Taking the root sum square of these errors, the revised lifetime is $34 \pm 14 \pm 9$ ps. This value is shorter than the previously reported value of $77 \pm 14 \pm 19$ ps [6], but is consistent with the other two experimental results given above.

VI. DISCUSSION

The obtained $\tau(2_1^+)$ for ^{16,18}C are summarized in Table I. In the case of ^{16}C, the three $\tau(2_1^+)$ values obtained are consistent with each other. We adopted the weighted mean of the three values by considering only the statistical errors. For the systematic errors, since they are comparable in all three cases, we adopted the largest value (26%) as the resultant systematic error. The $\tau(2_1^+)$ value for ^{16}C thus obtained is $18.3 \pm 1.4 \pm 4.8$ ps.

The $\tau(2_1^+)$'s determined in the present work correspond to $B(E2)$ values of $2.6 \pm 0.2 \pm 0.7\, e^2$ fm^4 and $4.3 \pm 0.2 \pm 1.0\, e^2$ fm^4 for ^{16,18}C, respectively. Although the $B(E2)$ value for ^{18}C is almost twice as large as that of ^{16}C, it is comparable to the $B(E2) = 3.7\, e^2$ fm^4 of the closed-shell ^{14}C nucleus. Both the energy of the 2_1^+ state and the $B(E2)$ value remain small in ^{18}C, clearly indicating that the phenomenon of hindered $E2$ strength observed in ^{16}C persists in ^{18}C.

In Fig. 12(a), the $B(E2)$ values obtained for ^{16,18}C are compared with all known $B(E2)$ values for the even-even nuclei with $A < 50$ [38]. Nuclei with open shells tend to have $B(E2)$ values greater than 10 W.u., whereas nuclei with neutron- or/and proton shell closure tend to have distinctly smaller $B(E2)$ values. Typical examples of the latter category are the doubly magic nuclei, ^{16}O and ^{48}Ca, for which the $B(E2)$ values are known to be 3.17 and 1.58 W.u., respectively. The present $B(E2)$ values for ^{16,18}C are 1.1 and 1.5 W.u., respectively, which are even more suppressed than those of the doubly magic nuclei although they are supposed to be open-shell nuclei.

TABLE I. Summary of the mean lifetimes of the 2_1^+ states in ^{16}C and ^{18}C, and the corresponding $B(E2)$ values.

	$\tau(2_1^+)$	$B(E2)$	
	[ps]	[e^2fm^4]	[W.u.]
^{18}C	$18.9 \pm 0.9 \pm 4.4$	$4.3 \pm 0.2 \pm 1.0$	$1.5 \pm 0.1 \pm 0.4$
^{16}C[a]	$17.7 \pm 1.6 \pm 4.6$	$2.7 \pm 0.2 \pm 0.7$	$1.1 \pm 0.1 \pm 0.3$
^{16}C[b]	$19.6 \pm 3.0 \pm 4.5$	$2.4 \pm 0.4 \pm 0.6$	$1.0 \pm 0.2 \pm 0.2$
^{16}C[c]	$34 \pm 14 \pm 9$	$1.4 \pm 0.6 \pm 0.4$	$0.6 \pm 0.2 \pm 0.2$

[a]Inelastic channel at 72 MeV/nucleon.
[b]Breakup channel at 79 MeV/nucleon.
[c]Inelastic channel at 40 MeV/nucleon.

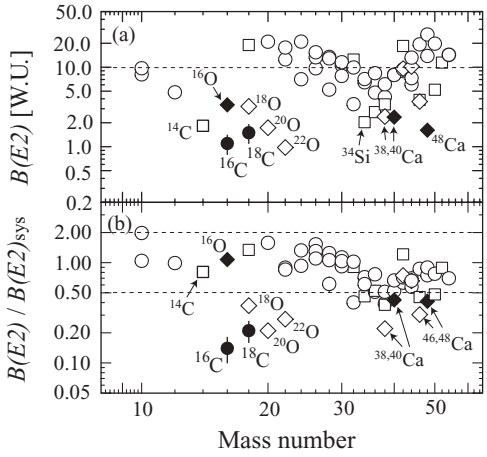

FIG. 12. (a) $B(E2)$ values in W.u. and (b) ratios between the experimental $B(E2)$ values and $B(E2)_{\rm sys}$ calculated using the empirical formula [8] for even-even nuclei with $A \leqslant 50$. The filled circles denote the values of ^{16,18}C, and the open circles represent data for other open-shell nuclei. The open squares and open diamonds denote the proton- and neutron-closed-shell nuclei, while the filled diamonds represent the double magic nuclei. The dashed lines are intended to guide the eye.

The strong hindrance of the ^{16,18}C transition can also be illustrated through comparison with an empirical formula based on a liquid-drop model [8]. The empirical formula can be expressed by

$$B(E2)_{\rm sys} = 6.47 \times Z^2 A^{-0.69} E(2_1^+)^{-1}.$$

The experimental $B(E2)$ values relative to $B(E2)_{\rm sys}$ are plotted in Fig. 12(b). As noted in Ref. [38], the $B(E2)/B(E2)_{\rm sys}$ ratios for most of the open-shell nuclei fall around 1.0, being confined between 0.5 and 2.0. Even for the closed-shell nuclei, the ratio remain larger than 0.20. Thus, the ratios of 0.14 and 0.21 for ^{16,18}C are exceptionally small. In particular, the ratio for ^{14}C with $E(2_1^+) = 7012$ keV [21] is as large as 0.68, suggesting different mechanisms for the small $B(E2)$ in ^{14}C and the suppression of the $B(E2)$ values in ^{16,18}C. As in the case of ^{16}C [9,10], the observation of the small $B(E2)$ value in ^{18}C despite the lowering of the $E(2_1^+)$ may imply a neutron-dominant quadrupole collectivity in ^{18}C.

Regarding the suppressed $B(E2)$ values for ^{16,18}C, calculations have been performed in several theoretical frameworks. Figure 13 shows the experimental and some of the theoretical $B(E2)$ values for carbon isotopes from ^{14}C to ^{20}C.

Calculations using the antisymmetrized molecular dynamics (AMD) [16,17] and the multi-Slater determinant AMD (AMD+MSD) [39] have reproduced the trend of the small $B(E2)$ values in ^{16,18}C. In the framework of the AMD calculation, the presence of opposite deformations in the neutron and proton are said to be accounted for the small $B(E2)$ in the ^{16,18}C isotopes. Meanwhile, another calculation using the deformed Hartree-Fock wave function [40] has reproduced the $B(E2)$ values in ^{16,18}C rather well, although

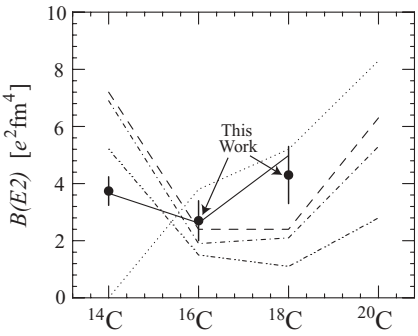

FIG. 13. Experimental $B(E2)$ for $^{14-20}$C isotopes (filled circles) in comparison with the $B(E2)$ predicted by theoretical calculations with the shell model [15] (dashed line), the AMD [17] (dash-dotted line), the AMD+MSD [39] (dash-double-dotted line), the deformed Skyrme Hartree-Fock [40] (dotted line), and the "no-core" shell model [41] (solid line).

it fails to reproduce the one in the neutron-closed-shell nucleus ^{14}C.

The shell model calculations [15,41] have also predicted suppressed $B(E2)$ values for ^{16,18}C. In the case of the calculation using a Hamiltonian with the strengthened tensor interaction [15], the energy gap between $(\pi 0p_{1/2})$-$(\pi 0p_{3/2})$ becomes as large as the gap for $(\pi 1s_{1/2})$-$(\pi 0p_{1/2})$, when the neutron number is 8 and 10. This large gap reduces the proton matrix element. As a result, the $0^+_{\mathrm{g.s.}} \rightarrow 2^+_1$ transition is mainly contributed by the neutrons. On the other hand, the dominant configuration of the valence neutrons in the sd-shell is $1s_{1/2}$, and since the valence neutrons in the s-orbit spread out widely, the effective charges become small. In fact, the effective charge of neutron has been calculated to be $e_n = 0.2e$ [12], which is smaller than the standard value $e_n = 0.5e$ used for the sd-shell nuclei. The other shell model calculation of the no-core type has reproduced successfully the present $B(E2)$ values for ^{16,18}C with a small neutron effective charge of $0.164e$ [41]. In the calculation, a quenched proton transition is expected. The occupation numbers of proton in the $0p_{3/2}$ orbits change by less than 1% for the ground and the 2^+_1 states in ^{16}C [41] and ^{18}C [42]. Thus, these two calculations give the same picture for the suppressed $B(E2)$ value. Note that the former shell model calculation predicts that the energy gap of $(\pi p_{1/2})$-$(\pi p_{3/2})$ decreases from ^{16}C to ^{22}C. As a result, proton matrix element will be enhanced, leading to larger $B(E2)$ values for ^{20,22}C.

While the above theoretical models offer possible interpretation for the hindered $E2$ transitions observed in ^{16,18}C, more theoretical and experimental studies on the ground states and other excited states, e.g. 2^+_1 state in ^{20}C, are necessary for a more unified and complete understanding of the structure of the neutron-rich carbon isotopes.

Finally, we comment on the experimental results of ^{16}C reported in Refs. [9,10]. A smaller $B(E2)$ value consistent with the one in Ref. [6] was reported in Ref. [9]. The underestimation of the $B(E2)$ value in Ref. [9] may indicate the need for a microscopic approach in analyzing the reaction data. In fact, a subsequent analysis [43] using the AMD wave functions [17] in the microscopic coupled-channels calculations has indicated a larger $B(E2)$ value of 1.9 e^2 fm^4. As for the work on the inelastic proton scattering on ^{16}C [10], the quadrupole deformation length was extracted from the experiment data. Using this deformation length and the $B(E2)$ value in Ref. [6], the ratio of the neutron and proton quadrupole matrix elements $(M_n/M_p)/(N/Z)$ was determined to be 4.0 ± 0.8. With the present $B(E2)$ value, the $(M_n/M_p)/(N/Z)$ value for ^{16}C becomes 1.9 ± 0.4, which is still very large and comparable to the value of ^{20}O [44]. In fact, the M_n value of about 11 fm^2 deduced for ^{16}C remains much larger than the M_p $(= \sqrt{5B(E2)/e^2})$ value, which was deduced to be about 4 fm^2 using the present $B(E2)$ value.

VII. SUMMARY

The lifetime of the 2^+_1 state in ^{16,18}C were successfully measured using the upgraded RSM with ten-layer NaI(Tl) array, incorporating the inelastic scattering and breakup reaction at around 75 MeV/nucleon. The γ-ray angular distribution for the inelastic scattering of ^{16}C at 40 MeV/nucleon was also measured. Incorporating this angular distribution into the measurement reported previously [6], the $\tau(2^+_1)$ of ^{16}C was found to be in consistent with the present result. The $\tau(2^+_1)$ values for ^{16,18}C thus determined were as long as around 20 ps, indicating that the anomalous suppression of $B(E2)$ observed in ^{16}C persists in ^{18}C. In the framework of shell model calculation, the suppressed $B(E2)$ values can be attributed to the small effective charges and the widening of the energy gap between the $\pi(p_{1/2})$-$\pi(p_{3/2})$ orbitals. The present results, together with the small $B(E2)$ values for ^{14}C, suggest a possible proton-shell closure in the neutron-rich ^{14,16,18}C nuclei.

ACKNOWLEDGMENTS

We thank the RIKEN Ring Cyclotron staff for the stable ^{22}Ne beam throughout the experiment. We acknowledge fruitful discussions with S. Fujii. H.J.O. is grateful to the Japan Society for the Promotion of Science for support. One of the authors (H.I.) would like to acknowledge support from the Alexander von Humboldt foundation. This work was supported in part by Grant-in-Aid for Scientific Research No. 15204017 from the Ministry of Education, Culture, Sports, Science and Technology of Japan.

[1] I. Tanihata *et al.*, Phys. Rev. Lett. **55**, 2676 (1985).
[2] T. Suzuki *et al.*, Phys. Rev. Lett. **75**, 3241 (1995).
[3] H. Iwasaki *et al.*, Phys. Lett. **B491**, 8 (2000).
[4] T. Motobayashi *et al.*, Phys. Lett. **B346**, 9 (1995).
[5] H. Scheit *et al.*, Phys. Rev. Lett. **77**, 3967 (1996).
[6] N. Imai *et al.*, Phys. Rev. Lett. **92**, 062501 (2004).
[7] A. Bohr and B. R. Mottelson, Mat. Fys. Medd. K. Dan. Vidensk. Selsk. **27**, No. 16 (1953); L. Grodzins, Phys. Lett. **2**, 88 (1962).
[8] S. Raman, C. W. Nestor, Jr., and K. H. Bhatt, Phys. Rev. C **37**, 805 (1988).
[9] Z. Elekes *et al.*, Phys. Lett. **B586**, 34 (2004).
[10] H. J. Ong *et al.*, Phys. Rev. C **73**, 024610 (2006).

[11] A. Bohr and B. R. Mottelson, *Nuclear Structure*, Vol. I (W. A. Benjamin, New York, 1969).
[12] H. Sagawa and K. Asahi, Phys. Rev. C **63**, 064310 (2001).
[13] H. Izumi *et al*., Phys. Lett. **B366**, 51 (1996).
[14] H. Ogawa *et al*., Phys. Rev. C **67**, 064308 (2003).
[15] R. Fujimoto, Ph.D. thesis, University of Tokyo, 2003.
[16] Y. Kanada-En'yo and H. Horiuchi, Phys. Rev. C **55**, 2860 (1997).
[17] Y. Kanada-En'yo, Phys. Rev. C **71**, 014310 (2005).
[18] Y. Suzuki, H. Matsumura, and B. Abu-Ibrahim, Phys. Rev. C **70**, 051302(R) (2004).
[19] W. Horiuchi and Y. Suzuki, Phys. Rev. C **73**, 037304 (2006).
[20] K. Hagino and H. Sagawa, Phys. Rev. C **75**, 021301(R) (2007).
[21] R. B. Firestone and V. S. Shirley, *Table of Isotopes*, 8th ed. (Wiley, New York, 1996), Vol. I.
[22] M. Staniou *et al*., Nucl. Phys. **A746**, 135c (2004).
[23] P. Limkilde and G. Sletten, Nucl. Phys. **A199**, 504 (1973).
[24] V. Metag, E. Liukkonen, G. Sletten, O. Glomset, and S. Bjørnholm, Nucl. Instrum. Methods **114**, 445 (1974).
[25] J. P. Bocquet *et al*., Phys. Lett. **B182**, 146 (1986).
[26] E. Gueorguieva, M. Kaci, C. Schück, A. Minkova, Ch. Vieu, J. J. Correia, and J. S. Dionisio, Nucl. Instrum. Methods A **474**, 132 (2001).
[27] L. C. Biedenharn, in *Nuclear Spectroscopy Part B*, edited by F. Ajzenberg Selove (Academic Press, New York, 1960); R. M. Diamond, E. Matthias, J. O. Newton, and F. S. Stephens, Phys. Rev. Lett. **16**, 1205 (1966) .
[28] D. Suzuki *et al*., submitted to Phys. Lett. B.
[29] T. Kubo *et al*., Nucl. Instrum. Methods B **70**, 309 (1992).
[30] I. Hisanaga, T. Motobayashi, and Y. Ando, RIKEN Accel. Prog. Rep. **31**, 162 (1998).
[31] T. Nishio *et al*., RIKEN Accel. Prog. Rep. **29**, 184 (1996).
[32] S. Takeuchi, T. Motobayashi, H. Murakami, K. Demichi, and H. Hasegawa, RIKEN Accel. Prog. Rep. **36**, 148 (2003).
[33] Program code GEANT, CERN program library.
[34] Z. Elekes *et al*., Phys. Lett. **B614**, 174 (2005).
[35] J. Raynal, coupled channel code ECIS79, unpublished.
[36] C.-C. Sahm *et al*., Phys. Rev. C **34**, 2165 (1986).
[37] Mariá-Ester Brandan, Phys. Rev. Lett. **60**, 784 (1988).
[38] S. Raman, C. W. Nestor, Jr., and P. Tikkanen, At. Data Nucl. Data Tables **78**, 1 (2001).
[39] G. Thiamova, N. Itagaki, T. Otsuka, and K. Ikeda, Eur. Phys. J. A **22**, 461 (2004).
[40] H. Sagawa, X. R. Zhou, X. Z. Zhang, and T. Suzuki, Phys. Rev. C **70**, 054316 (2004).
[41] S. Fujii, T. Mizusaki, T. Otsuka, T. Sebe, and A. Arima, Phys. Lett. **B650**, 9 (2007).
[42] S. Fujii, private communication.
[43] M. Takashina, Y. Kanada-En'yo, and Y. Sakuragi, Phys. Rev. C **71**, 054602 (2005).
[44] J. K. Jewell *et al*., Phys. Lett. **B454**, 181 (1999); E. Khan *et al*., *ibid*. **B490**, 45 (2000).